Structural and Electrochemical Characterization of the $LiNi_{1-y}Ti_yO_2$ Electrode Materials Obtained by Direct Solid-State Reactions

L. Croguennec,*,† E. Suard,‡ P. Willmann,§ and C. Delmas†

Institut de Chimie de la Matière Condensée de Bordeaux-CNRS and Ecole Nationale Supérieure de Chimie et Physique de Bordeaux, 87, Avenue du Dr A. Schweitzer, 33608 Pessac Cedex, France, Institut Laue-Langevin, Avenue Jules Horowitz, BP 156, 38042 Grenoble Cedex 9, France, and CNES, 18 Avenue Edouard Belin, 31055 Toulouse Cedex, France

Received October 26, 2001. Revised Manuscript Received February 20, 2002

$LiNi_{1-y}Ti_yO_2$ ($y \leq 0.15$) layered oxides were synthesized at high temperature by solid-state reactions. Rietveld refinements of their X-ray and neutron diffraction patterns showed that these phases were characterized by an α-$NaFeO_2$-type structure with the following cationic distribution: $(Li_{1-z}Ni^{2+}_z)_{3b}(Ti^{4+}_tNi^{2+}_{t+z}Ni^{3+}_{1-z-2t})_{3a}O_2$ [$t = y(1 + z)$]. The amount of Ni^{2+} ions in the lithium site increases with y. A magnetic study confirmed the presence of paramagnetic ions in the interslab space and, therefore, the cationic distribution. These materials used as positive electrode in lithium batteries show reversible behavior. A large decrease of the capacity is observed with increasing y, because of the presence of extra nickel ions in the lithium sites. For the "$Li_xNi_{0.95}Ti_{0.05}O_2$" composition, 144 mA h/g are obtained in discharge at the 14th cycle at the $C/20$ rate. The "$Li_xNi_{1-y}Ti_yO_2$" phases were characterized for $y = 0.05$ and 0.10: the simultaneous presence of titanium ions in the slab and of a significant amount of extra nickel ions in the lithium sites prevents phase transitions upon cycling.

1. Introduction

Layered lithiated transition metal oxides, such as $LiCoO_2$ and $LiNiO_2$, are attractive as positive electrode materials for lithium-ion batteries.[1−6] Recently, $LiNiO_2$ has been largely studied because of the comparatively low cost of nickel versus cobalt. However, because of the thermal instability of Li_xNiO_2 in the very oxidized state, which is characterized by a sharper exothermic reaction at a lower temperature than Li_xCoO_2,[7] $LiCoO_2$ still remains the most-used positive electrode material in commercial lithium-ion batteries.

Recent studies have shown that cationic substitution for nickel appears to be a good way to modify the structural and electrochemical properties of lithium nickelate. For instance, it was shown that a partial substitution of cobalt for nickel increases the lamellar character of the lithium nickelate inducing a better reversibility of the Li||$Li_x(Ni,Co)O_2$ system,[8−10] whereas a substitution of magnesium for nickel leads to an improvement of the stability of the Li||$Li_x(Ni,Mg)O_2$ system upon cycling.[11,12] An increase of the thermal stability of $LiNiO_2$ in the oxidized state has also been achieved through the substitution of aluminum,[13] manganese[14,15] or titanium[14−16] for nickel. Cosubstituted nickelate compounds such as $LiNi_{1-x}Ti_{x/2}Mg_{x/2}O_2$[17] and $LiNi_{0.8}Co_{0.1}Ti_{0.1}O_2$[15] have also been proposed as materials exhibiting large capacities, good cyclabilities, and good thermal stabilities in the delithiated state.

In this study, titanium-substituted lithium nickelate $LiNi_{1-y}Ti_yO_2$ ($0 < y \leq 0.15$) phases were synthesized and characterized from the structural, magnetic, and electrochemical points of view. This study is, in fact, the first step necessary before attempts can be made to

* Corresponding author. Phone: (+33) 5-5796-2234. Fax: (+33) 5-5684-6698. E-mail: crog@icmcb.u-bordeaux.fr.

† Institut de Chimie de la Matière Condensée de Bordeaux-CNRS and Ecole Nationale Supérieure de Chimie et Physique de Bordeaux.

‡ Institut Laue-Langevin.

§ CNES.

(1) Thomas, M. G. S. R.; David, W. I. F.; Goodenough, J. B.; Groves, P. *Mater. Res. Bull.* **1985**, *20*, 1137.

(2) Dahn, J. R.; von Sacken, U.; Juzkow, M. W.; Al-Janaby, H. *J. Electrochem. Soc.* **1991**, *138*, 2207.

(3) Broussely, M.; Perton, F.; Labat, J.; Staniewicz, R. J.; Romero, A. *J. Power Sources* **1993**, *43−44*, 209.

(4) Broussely, M.; Perton, F.; Biensan, P.; Bodet, J. M.; Labat, J.; Lecerf, A.; Delmas, C.; Rougier, A.; Pérès, J. P. *J. Power Sources* **1995**, *54*, 109.

(5) Ohzuku, T.; Ueda, A. *J. Electrochem. Soc.* **1994**, *141*, 2972.

(6) Rougier, A.; Gravereau, P.; Delmas, C. *J. Electrochem. Soc.* **1996**, *143*, 1168.

(7) Dahn, J. R.; Fuller, E. W.; Obrovac, M.; von Sacken, U. *Solid State Ionics* **1994**, *69*, 265.

(8) Saadoune, I.; Delmas, C. *J. Mater. Chem.* **1996**, *6*, 193.

(9) Rougier, A.; Saadoune, I.; Gravereau, P.; Willmann, P.; Delmas, C. *Solid State Ionics* **1996**, *90*, 83.

(10) Zhecheva, E.; Stoyanova, R. *Solid State Ionics* **1993**, *66*, 143.

(11) Pouillerie, C.; Croguennec, L.; Biensan, P.; Willmann, P.; Delmas, C. *J. Electrochem. Soc.* **2000**, *147*, 2061.

(12) Pouillerie, C.; Croguennec, L.; Delmas, C. *Solid State Ionics* **2000**, *132*, 15.

(13) Ohzuku, T.; Yanagawa, T.; Kouguchi, M.; Ueda, A. *J. Power Sources* **1997**, *68*, 131.

(14) Arai, H.; Okada, S.; Sakurai, Y.; Yamaki, J. *J. Electrochem. Soc.* **1997**, *144*, 3117.

(15) Arai, H.; Tsuda, M.; Sakurai, Y. *J. Power Sources* **2000**, *90*, 76.

(16) Kim, J.; Amine, K. *Electrochem. Commun.* **2001**, *3*, 52.

(17) Gao, Y.; Yakovleva, M. V.; Ebner, W. B. *Electrochem. Solid-State Lett.* **1998**, *1*, 117.

10.1021/cm011265v CCC: $22.00
Published on Web 04/19/2002

Table 1. Experimental Conditions Used for the Synthesis of the $LiNi_{1-y}Ti_yO_2$ Phases ($y = 0.02$, 0.05, 0.10, and 0.15)[a]

$[Ti/(Ti + Ni)]_{nominal}$	synthesis conditions	$I_{(003)}/I_{(104)}$[a]
0.02	800 °C, 12 h, O_2	1.01
0.05	850 °C, 24 h, O_2	1.05
0.10	850 °C, 32 h, O_2	0.74
0.15	850 °C; 32 h; O_2, grinding, 870 °C; 32 h; O_2	0.49

[a] The $I_{(003)}/I_{(104)}$ X-ray diffraction line intensity ratios are also given for comparison.

understand the mechanisms that are at the origin of the reported thermal stabilization of these titanium-substituted lithium nickelates in the highly oxidized state.

2. Experimental Section

Polycrystalline samples of composition $LiNi_{1-y}Ti_yO_2$ ($0.02 \leq y < 0.20$) were prepared by direct solid-state reactions using the appropriate amounts of Li_2O, NiO [obtained by decomposition of $Ni(NO_3)_2$ at 450 °C], and TiO_2 anatase. An excess amount of lithium oxide (5 mol %) was added to compensate for the loss because of the volatilization of the lithium component at high temperature. The mixture was ground in an argon-filled drybox and then heated as reported in Table 1 under an oxygen gas flow. The heating and cooling rates were controlled at 1 and 2 °C/min, respectively. For all of the materials, chemical analyses were performed by ICP (inductively coupled plasma) absorption spectroscopy.

Identification of crystalline phases and determination of their structures were carried out by X-ray and neutron powder diffraction analyses. The X-ray diffraction (XRD) study was performed using a Siemens D5000 diffractometer (reflection mode) with Cu Kα radiation. Data were collected using a step-scanning mode in the 2θ range of 5−120° with a step width of 0.02° and a step time of 40 s. The neutron diffraction data were recorded on high-resolution powder diffractometer D2B of the Institut Laue-Langevin. The samples were contained in a vanadium tube with a diameter of 8 mm. The diffraction patterns ($\lambda = 1.594$ Å) were collected at room temperature from 0° to 162° (2θ) with a 0.05° (2θ) step and a total counting time of 6 h. All crystal structures were refined by the Rietveld method using the Fullprof 2000 program.[18] Because of the geometry of the neutron diffractometer (transmission mode), it was necessary to correct for the absorption to take into account a decrease of the experimental diffracted intensity compared to the expected one. This correction is all the more necessary because these samples contain lithium, which is quite absorbent in neutron diffraction. This correction (through the μR factor in the Fullprof program) is especially necessary for the determination of the atomic displacement parameters and site occupancies that strongly depend on the intensities of the diffraction lines. μ is the linear absorption coefficient of the sample and is defined as $\mu = (n/V)\Sigma n_i \sigma_{ai}$, where n is the number of units in the unit cell, V is the cell volume, n_i is the number of atoms of type i in the unit cell, and σ_{ai} is the atomic absorption coefficient for atoms of type i. R is the radius of the cylinder defined by the studied sample. The calculated μR coefficients for the two phases $LiNi_{0.95}Ti_{0.05}O_2$ and $LiNi_{0.85}Ti_{0.15}O_2$ were 0.73 and 0.77, respectively.

Magnetization was measured at 5 K using a SQUID magnetometer (Quantum Design, MPMS-5S). A hysteresis cycle was performed in the field range from −2000 to +2000 G with a 100 G step.

Electrochemical experiments were carried out in lithium cells with the following configuration: Li|1 M $LiPF_6$ in propylene carbonate (PC), ethylene carbonate (EC), dimethyl carbonate (DMC) (1:1:3)|$Li_xNi_{1-y}Ti_yO_2$. The positive electrodes were prepared from a mixture of 88 wt % $LiNi_{1-y}Ti_yO_2$ (25 mg), 10 wt % carbon black as the conductive agent, and 2 wt % poly(tetrafluoroethylene) (PTFE) as the binder. Cells were assembled in an argon-filled drybox and cycled at room temperature using a homemade system monitored by an HP1000 computer operating in the galvanostatic mode.[19] The electrochemical performances of the various compounds were evaluated upon cycling in the 3.0−4.6 V potential range at the $C/20$ or $C/100$ rate, the C rate being here defined as the exchange of 1 electron in 1 h. The delithiated samples were prepared electrochemically. They were recovered in a glovebox, washed in DMC to remove the remaining $LiPF_6$ salt and dried under vacuum. For the X-ray diffraction study, a sample holder that avoided any contact of the oxidized positive electrodes with air was used.

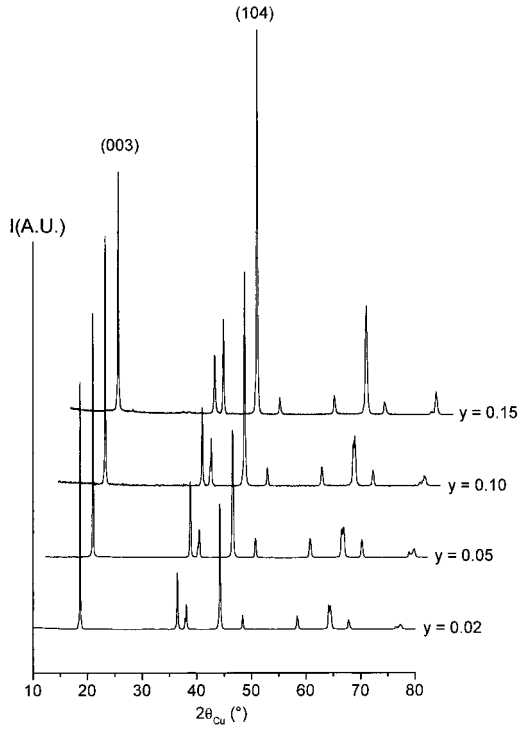

Figure 1. X-ray diffraction patterns of the $LiNi_{1-y}Ti_yO_2$ phases ($y = 0.02$, 0.05, 0.10, and 0.15). The patterns were shifted for clarity of presentation; only the $y = 0.02$ XRD pattern is not shifted.

3. Results and Discussion

3.1. Structural Characterization of the $LiNi_{1-y}Ti_yO_2$ Phases. Single phases isostructural to $LiNiO_2$ were obtained for $LiNi_{1-y}Ti_yO_2$ with $0.02 \leq y \leq 0.15$. The evolution of the XRD patterns of these materials with y is shown in Figure 1. The XRD lines are quite narrow for all of the samples, which indicates a quite good homogeneity and crystallinity of the materials. This result is in agreement with the SEM observation, which shows ill-defined shapes but with a homogeneous size distribution (~1 μm).

Traces of Li_2CO_3 are observed, because of the excess of lithium precursor in the starting mixtures. In all cases, the Ni/Ti ratio was confirmed by chemical analysis, but because of the presence of a small amount of Li_2CO_3 in all of the samples, the data thus obtained did not allow for the precise determination of the actual chemical formulas of the $LiNi_{1-y}Ti_yO_2$ compounds.

(18) Rodriguez-Carvajal, J., Laboratoire Léon Brillouin (CEA-CNRS), http://www-llb.cea.fr/fullweb/powder.htm.

(19) Mendiboure, A.; Delmas, C. *Comput. Chem.* **1987**, *11*, 153.

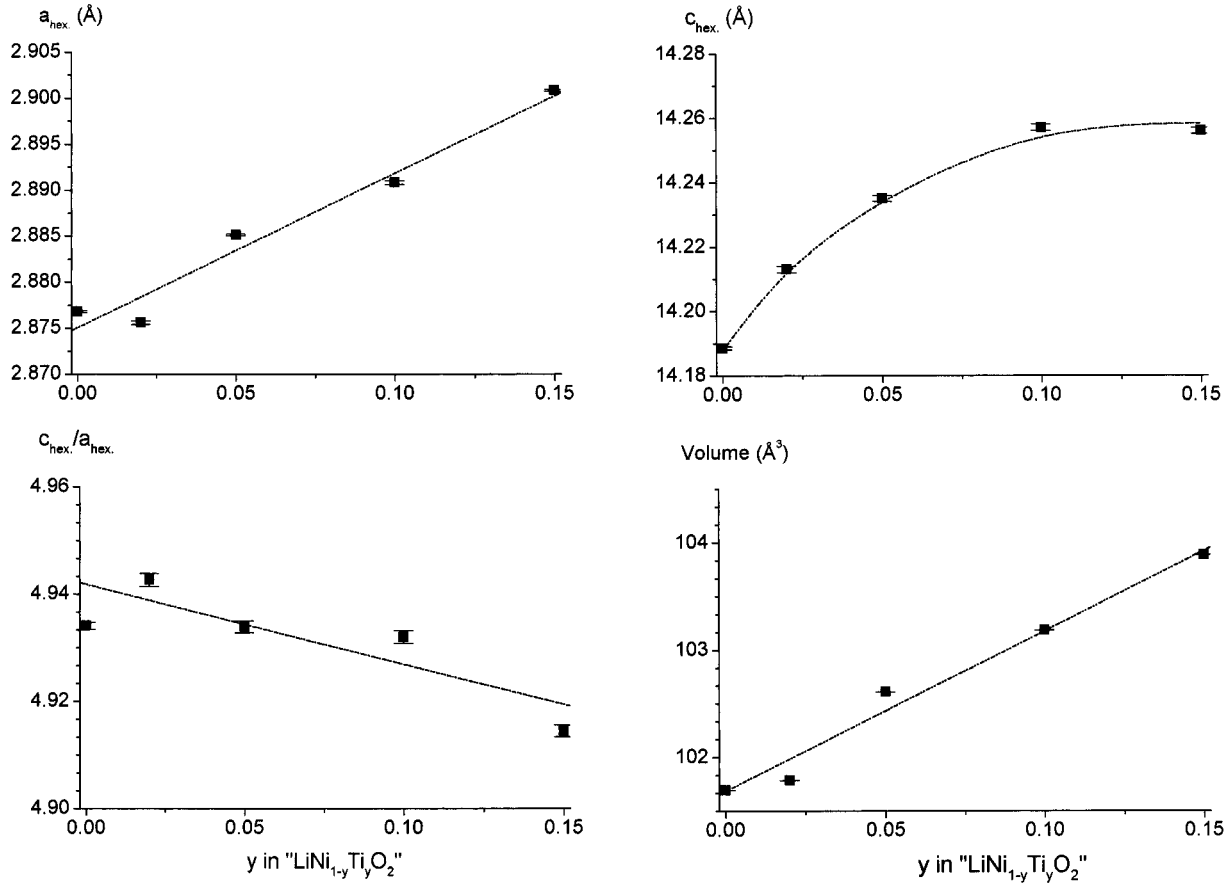

Figure 2. Variation of the structural parameters (a_{hex}, c_{hex}, c_{hex}/a_{hex}, and volume) versus y in the $LiNi_{1-y}Ti_yO_2$ phase.

Table 2. Structural Parameters and Crystallographic Formulas Determined by Rietveld Refinement of the X-ray and Neutron Diffraction Patterns of the $LiNi_{1-y}Ti_yO_2$ Phases (y = 0.00, 0.02, 0.05, 0.10, and 0.15)

compound	diffraction method	a_{hex} (Å)	c_{hex} (Å)	z_{ox}	z	crystallographic formula	R_{wp} (%)	R_B (%)
$LiNiO_2$	XRD	2.8768(1)	14.188(1)	0.2585(2)	0.022(6)	$[Li_{0.98}Ni_{0.02}][Ni]O_2$	9.80	2.60
$LiNi_{0.98}Ti_{0.02}O_2$	XRD	2.8756(2)	14.213(1)	0.2579(4)	0.020(6)	$[Li_{0.98}(Ti_{0.02}Ni_{0.98})_{0.02}][Ti_{0.02}Ni_{0.98}]O_2$	9.40	3.40
$LiNi_{0.95}Ti_{.05}O_2$	XRD	2.8856(1)	14.239(1)	0.2574(4)	0.080(6)	$[Li_{0.92}(Ti_{0.05}Ni_{0.95})_{0.08}][Ti_{0.05}Ni_{0.95}]O_2$	12.0	3.06
	neutron	2.8851(1)	14.235(1)	0.2581(2)	0.072(6)	$[Li_{0.93}Ni_{0.07}][Ti_{0.05}Ni_{0.95}]O_2$	13.1	3.64
$LiNi_{0.90}Ti_{0.10}O_2$	XRD	2.8908(2)	14.257(1)	0.2568(5)	0.120(6)	$[Li_{0.88}(Ti_{0.10}Ni_{0.90})_{0.12}][Ti_{0.10}Ni_{0.90}]O_2$	9.64	1.72
$LiNi_{0.85}Ti_{0.15}O_2$	XRD	2.9008(2)	14.261(1)	0.2561(7)	0.227(6)	$[Li_{0.77}(Ti_{0.15}Ni_{0.85})_{0.23}][Ti_{0.15}Ni_{0.85}]O_2$	12.0	3.44
	neutron	2.9008(2)	14.256(1)	0.2556(3)	0.239(6)	$[Li_{0.76}Ni_{0.24}][Ti_{0.19}Ni_{0.81}]O_2$	16.5	5.53

With an increase in the substitution of titanium for nickel, it appears that an increase of the thermal treatment temperature is required for pure single-phase samples to be obtained (Table 1). However, high temperatures favor the formation of phases characterized by a large lithium deficiency. Note, for instance, that the (003)/(104) diffraction line intensity ratio is very small for $LiNi_{0.85}Ti_{0.15}O_2$ (about 0.5, as reported in Table 1), in comparison with the value close to 1.3 observed for a highly ordered $LiNiO_2$ phase. Furthermore, for all of the samples, the (018)/(110) doublet is not well separated. These two last points concerning specific XRD lines provide, in lithium nickelates, evidence for the degree of disorder and lithium deficiency and, therefore, for the presence of transition metal in the interslab space.[6]

Note that, for titanium-rich compositions ($y > 0.15$), the synthesis of a single-phase compound was unsuccessful, regardless of the thermal treatment temperature (≤900 °C) and reaction time used. Syntheses with higher reaction temperatures were shown to favor a lithium deficiency because of the high vapor pressure of lithium oxide at such temperatures and, therefore, to favor the formation of highly disordered phases, which crystallize in the cubic system (with a rock-salt structure close to that of NiO). No improvement of the synthesis conditions was obtained through the use of pressed pellets or other precursors for lithium. Note that the coprecipitation method was not used because of the lack of inexpensive precursors for titanium.

3.1.1. X-ray and Neutron Diffraction Analysis of the Layered $LiNi_{1-y}Ti_yO_2$ Phases. X-ray Diffraction Analysis. The $LiNi_{1-y}Ti_yO_2$ materials were first characterized by a full-pattern-matching refinement of their cell parameters (profile fitting procedure from the Fullprof program that does not require any structural model but only constrains the angular position of the reflections to be consistent with the cell parameters and refines the shapes of the diffraction lines). A general comparison of these data for all samples is given in Table 2 and Figure 2. An increase of the a_{hex} and c_{hex} parameters with increasing y is observed, because of the larger size of the titanium ions ($r_{Ti^{4+}} = 0.605$ Å) compared to the Ni^{3+} ions (0.56 Å).[20] Furthermore, the c_{hex}/a_{hex} ratio

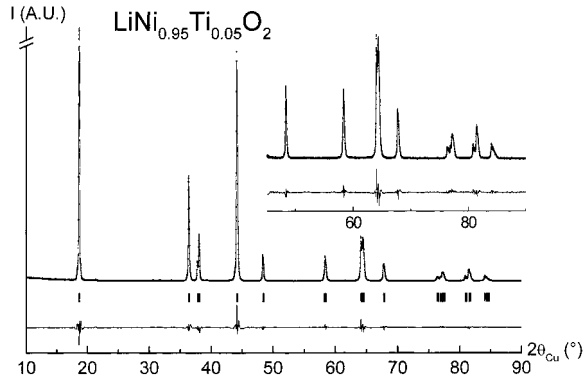

Figure 3. Comparison of the experimental (●) and calculated (—) X-ray diffraction profiles for $LiNi_{0.95}Ti_{0.05}O_2$. The difference and the positions of the (*hkl*) lines are also provided.

decreases with increasing y and approaches the 4.90 theoretical value for cubic symmetry; this indicates the tendency to form disordered phases characterized by lithium deficiency.

Rietveld refinement of the XRD patterns was carried out using the method described for the $Li_{1-z}Ni_{1+z}O_2$ system.[6] Indeed, as previously reported, the amount z of extra metal ions located in the lithium site can be determined by taking advantage of the strong correlation that exists between z and the B(Li) isotropic atomic displacement parameter.[6] For all of the $LiNi_{1-y}Ti_yO_2$ samples, if the Rietveld refinement is carried out assuming a perfectly ordered α-$NaFeO_2$-type structure ($z = 0$) with $(1 - y)$ Ni ions and y Ti ions in the 3a site (0, 0, 0) and 1 Li ion in the 3b site (0, 0, $^1/_2$) (space group $R\bar{3}m$), then a negative value is obtained for the B(Li) parameter [for instance, B(Li) = −1.8 Å^2 for $LiNi_{0.95}Ti_{0.05}O_2$]. This result provides evidence for an excess of electronic density in the lithium site that is not taken into account in such an ideal structural hypothesis and, therefore, for the presence of extra 3d transition metal in the lithium site. Because the X-ray scattering factors vary continuously with atomic number, there is a lack of contrast by XRD between elements that are close to each other in the periodic table. Similar agreements are obtained between the experimental and calculated XRD patterns if we make the hypothesis that the residual electronic density is due either to a single 3d transition metal (Ni or Ti) or to the undifferentiated presence of the two in the lithium site: only a slight modification of the site occupancy for the extra ion(s) is observed. Therefore, X-ray diffraction alone does not allow the nature of the extra 3d transition elements present in the lithium site to be determined. The results of the Rietveld refinement of the $LiNi_{1-y}Ti_yO_2$ XRD patterns are gathered in Table 2. The refinement was performed with two constraints: the total occupancy at each site was equal to 1, and the Ni/Ti ratio was equal to $(1 - y)/y$. A comparison of the experimental and calculated profiles is also shown for $LiNi_{0.95}Ti_{0.05}O_2$ in Figure 3. This phase was shown to be characterized by an 8% lithium deficiency. Note that a good minimization of the difference is observed, with good reliability factors R_{wp} and R_B.

Neutron Diffraction Analysis. The two phases "$LiNi_{0.95}Ti_{0.05}O_2$" and "$LiNi_{0.85}Ti_{0.15}O_2$" were studied by neutron diffraction. A neutron diffraction study was performed to overcome the weak points of XRD diffraction. Because the neutron scattering amplitude varies almost randomly throughout the periodic table, relatively close elements such as Ti and Ni have very different Fermi lengths [b(Ti) = -0.3438×10^{-12} cm and b(Ni) = 1.0300×10^{-12} cm], whereas they have very similar X-ray scattering factors [f(Ti) = 6.2×10^{-12} cm and f(Ni) = 7.9×10^{-12} cm, with sin $\theta = 0$]. Furthermore, the opposite signs of the nickel and titanium Fermi lengths should help to determine unambiguously the nature of the extra ion that is present in the lithium site. As illustrated in Figure 4, the neutron diffraction scattering amplitude in the lithium site is predicted to evolve in opposite ways according to the (Li, Ni) and (Li, Ti) hypotheses for the cationic distribution in the interslab space, whereas approximately the same evolution is observed in both cases by X-ray diffraction. Note that, by neutron diffraction, the scattering amplitude can be the same for some (Li, Ti, Ni) distributions at the lithium site and for lithium alone. In that case, a combined study by X-ray and neutron diffraction is required. Furthermore, a good knowledge of the chemical composition of the material and, therefore, of the total Ti/Ni ratio, certainly helps in the determination of the cationic distribution of these substituted lithium nickelate compounds, as it provides an additional constraint for the structural refinement by the Rietveld method.

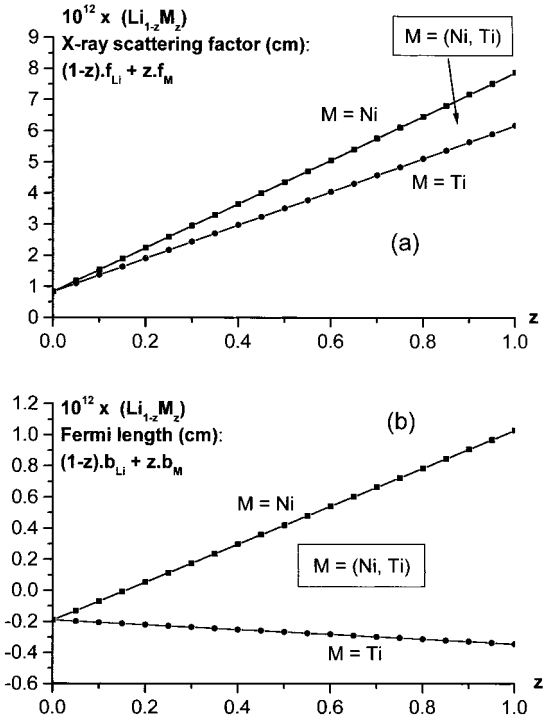

Figure 4. Evolution of the scattering amplitude in the 3b ($Li_{1-z}M_z$) site (with M = Ti or Ni) as determined by (a) X-ray diffraction and (b) neutron diffraction.

As in the case of XRD analyses, the structures of these compounds were first refined (space group $R\bar{3}m$) with Li, Ni (Ti), and O in the 3b (0, 0, $^1/_2$), 3a (0, 0, 0), and 6c (0, 0, z_{ox}) sites, respectively. The isotropic atomic displacement factors were fixed in the first step at 0.5 Å^2 (typical values obtained for that kind of element in such structure types). The refined cell and the oxygen position parameters were identical to those found in the

(20) Shannon, R. D.; Prewitt, C. T. *Acta Crystallogr.* **1969**, *B25*, 925.

Table 3. Parameters and Reliability Factors Obtained by the Rietveld Refinement of the Neutron Diffraction Pattern of $LiNi_{0.95}Ti_{0.05}O_2$

$LiNi_{0.95}Ti_{0.05}O_2$						
			constraints			
space group $R\bar{3}m$ $a_{hex} = 2.8851(1)$ Å $c_{hex} = 14.2347(6)$ Å			$n(Li) + n(Ni_1) = 1$ $B(Li) = B(Ni_1)$ $B(Ni_2) = B(Ti)$		$n(Ni_2) + n(Ti) = 1$	
atom	site		Wyckoff positions		B_{iso} (Å^2)	occupancy
Li	3b	0	0	0.5	1.5(6)	0.928(6)
Ni_1	3b	0	0	0.5	1.5(6)	0.072(6)
Ni_2	3a	0	0	0	0.59(6)	0.946(6)
Ti	3a	0	0	0	0.59(6)	0.054(6)
O	6c	0	0	0.2581(2)	0.67(6)	1
			U_{11} (Å^2)		U_{33} (Å^2)	U_{11}/U_{33}
(Ni_2, Ti) (3a)			0.006		0.010	0.6
O (6c)			0.011		0.004	2.75
(Ni_2,Ti)−O = 1.980(2) Å (×6)			(Li,Ni_1)−O = 2.114(2) Å (×6)			
$(O-O)_{slab}$ = 2.713(4) Å (×3)			$(O-O)_{interslab}$ = 3.090(4) Å (×3)			
conditions of the run						
wavelength					1.59406 Å	
temperature					300 K	
angular range					$-7.45° \le 2\theta \le 162°$	
step scan increment (2θ)					0.05°	
zero point (2θ)					0.012(3)	
number of fitted parameters					19	
profile parameters						
profile function pseudo-Voigt					$PV = \eta L + (1-\eta)G$	
$\eta = \eta_0 + X(2\theta)$					$\eta_0 = 0.22(5)$	
					$X = 0.0011(6)$	
half-width parameters					$U = 0.093(6)$	
					$V = -0.11(1)$	
					$W = 0.115(6)$	
conventional Rietveld R factors for points with Bragg contributions						
$R_{wp} = 13.1\%$					$R_B = 3.64\%$	
$(Li_{0.928}Ni^{2+}_{0.072})_{3b}(Ti^{4+}_{0.054}Ni^{2+}_{0.126}Ni^{3+}_{0.820})_{3a}O_2$						

XRD refinement (see Table 2). Then, a lithium deficiency, allowing either nickel or titanium to occupy the lithium site, was considered, with the constraint that the total occupancy at each site was equal to 1 and that the overall Ni/Ti ratio was equal to $(1 - y)/y$. The refinement showed that the 3b site contains lithium and nickel only, with the partial site occupancy associated with titanium being equal to zero. Moreover, the hypothesis assuming that the lithium deficiency is compensated by the presence of titanium leads to an unsatisfactory refinement. Finally, when the isotropic atomic displacement factors B were refined, no significant modifications of the structural parameters were observed. Note that, as the neutron diffraction technique considers only the average structure, a single atomic displacement parameter can be determined for a given site; B_{3b}, for example, is the atomic displacement parameter associated with an atom that has z% of nickel character and $(1 - z)$% of lithium character. The refinement of the neutron powder diffraction patterns for $LiNi_{0.95}Ti_{0.05}O_2$ and $LiNi_{0.85}Ti_{0.15}O_2$ showed that 7.2% and 23.9% extra nickel ions, respectively, were in the lithium site. The results of the refinement obtained for the $y = 0.05$ phase are gathered as an example in Table 3. The corresponding observed and experimental profiles are compared in Figure 5. Note that a good minimization of the difference is observed with good reliability factors R_{wp} and R_B. The isotropic atomic displacement parameter in the lithium site has a larger standard deviation. Indeed, because of its high absorption coefficient (natural lithium was used for the synthesis), its accurate observation remains difficult.

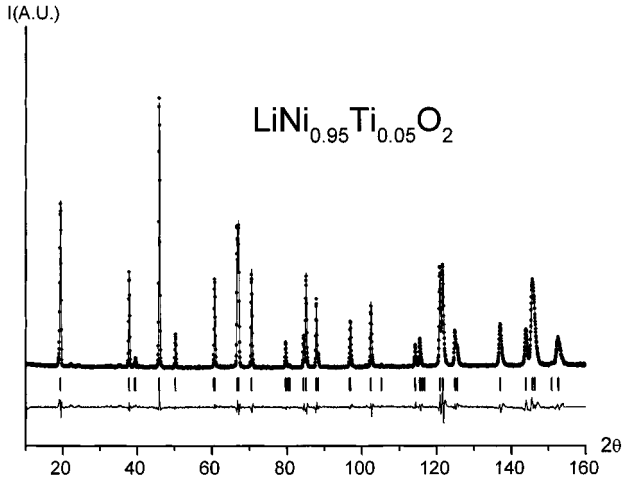

Figure 5. Comparison of the experimental (●) and calculated (—) neutron diffraction profiles for $LiNi_{0.95}Ti_{0.05}O_2$. The difference and the positions of the (hkl) lines are also provided.

The U_{ij} anisotropic displacement parameters related to the Ni (Ti) (3a) and O (6c) sites are also given in Table 3. In the rhombohedral lattice mode of trigonal symmetry, only the U_{11} and U_{33} parameters can be consid-

ered, where U_{11} and U_{33} describe the probability of displacement for the atoms in the $(a,b)_{hex}$ plane (parallel to the slab) and along the c_{hex} direction (perpendicular to the slab), respectively. In good agreement with the results obtained for $Li_{1-z}Ni_{1+z}O_2$ ($z = 0.07$),[21] quasi-isotropic displacements of the nickel (and titanium) ions in their octahedral sites and preferential displacements of the oxygen ions in the $(a,b)_{hex}$ plane are observed. Indeed, the presence of a significant amount of Ni^{2+} ions in the slab tends to distort the lattice locally, inducing a larger displacement of the surrounding oxygen ions in the $(a,b)_{hex}$ plane and, thus, an increase in the U_{11}(O)/U_{33}(O) ratio.

A partial disordering with extra nickel ions in the lithium site and lithium ions in the 3d metal layer was also considered with the constraints given above. The presence of lithium in the slab was not found to be significant, with less than 2% of lithium ions in the Ni(Ti)O_2 slab for the $y = 0.15$ phase and a very large standard deviation in this value. It appears that this large standard deviation reflects the fact that too many structural parameters have already been refined for the amount of information given by the neutron data. Furthermore, it should be pointed out that the negative coherent scattering length of Li [b(Li) $= -0.1900 \times 10^{-12}$ cm] is an advantage in the refinement of its amount in a NiO_2 slab because the nickel atom has a high positive b value [b(Ni) $= 1.0300 \times 10^{-12}$ cm]. However, because of the large negative b value of the Ti atom [b(Ti) $= -0.3438 \times 10^{-12}$ cm], partial substitution of titanium for nickel makes the refinement of the amount of Li in a Ni(Ti)O_2 slab less efficient.

These neutron diffraction analyses are in good agreement with the latter X-ray diffraction results, as 7.2 and 23.9% extra nickel ions were found in the lithium site, whereas 8 and 22.7% extra metal ions were found in the XRD study. As suggested by the variation of the $I_{(003)}/I_{(104)}$ ratio of the X-ray diffraction patterns, there is an increase in the lithium deficiency with increasing y.

Discussion of the Structural Results. The Rietveld refinement of the XRD and neutron diffraction data indicated the presence of only extra nickel ions in the lithium site and, as a consequence, of only titanium ions in the nickel site. From a general point of view, the formation of the $LiMO_2$-type structure results from the size difference between the LiO_6 and MO_6 octahedra, so the largest ions are expected to occupy the lithium site preferentially.

Under the synthesis conditions used in this study (TiO_2 as the precursor and oxidizing conditions), the titanium ions were assumed to be present in the 4+ oxidation state. Note, for instance, that $NaTiO_2$ is obtained only in a very reducing medium (under a high Na metal vapor pressure).[22,23]

Because of the difference in size between the Ti^{4+}, Ni^{3+}, and Li^+ ions [$r(Ti^{4+}) = 0.605$ Å, $r(Ni^{3+}) = 0.56$ Å, and $r(Li^+) = 0.72$ Å], the tetravalent titanium ions substitute for trivalent nickel ions in $LiNiO_2$ and induce the presence of an equal amount of Ni^{2+} ions in the slab for charge compensation. The larger sizes of the Ti^{4+} and Ni^{2+} ions versus Ni^{3+} tend to increase the M−O distance in the slab (Table 4) and, therefore, to destabilize the Ni^{3+} ions, as was also observed for the iron-substituted lithium nickelate phases.[24] This increase in Ni^{2+} ions in the slab induces an increasing amount of extra metal ions in the lithium site for charge compensation and, therefore, a larger lithium deficiency. Again, because of the difference in size between the Ti^{4+}, Ni^{3+}, Ni^{2+} [$r(Ni^{2+}) = 0.70$ Å], and Li^+ ions, it is justified to assume that the extra metal ions present in the lithium site are Ni^{2+} ions. The following cationic distribution is thus proposed for the $LiNi_{1-y}Ti_yO_2$ materials: $(Li_{1-z}Ni^{2+}_z)_{3b}(Ti^{4+}_t Ni^{2+}_{t+z} Ni^{3+}_{1-z-2t})_{3a}O_2$, with $t = y(1 + z)$, by just taking into account the difference in size between the different cations. Note that this cationic distribution is in very good agreement with the results obtained from the X-ray and neutron diffraction data.

Table 4. Average Nickel Oxidation Number and Interatomic Distances Calculated for the $LiNi_{1-y}Ti_yO_2$ Phases ($y = 0$, 0.02, 0.05, 0.10, and 0.15)

compound	y	average Ni oxidation number[a]	$d_{(Ni(Ti)-O)}$ (Å)[b]	$d_{(Li(Ni)-O)}$ (Å)[b]
$Li_{0.98}Ni_{1.02}O_2$	0	2.96	1.971(2)	2.111(2)
$Li_{0.98}(Ti_{0.02}Ni_{0.98})_{1.02}O_2$	0.02	–	1.976(2)	2.107(2)
$Li_{0.93}Ti_{0.05}Ni_{1.02}O_2$	0.05	2.81	1.980(2)	2.114(2)
$Li_{0.88}(Ti_{0.10}Ni_{0.90})_{1.12}O_2$	0.10	–	1.994(3)	2.107(3)
$Li_{0.76}Ti_{0.19}Ni_{1.05}O_2$	0.15	2.37	2.008(3)	2.101(3)

[a] Calculated from the cationic distribution determined by the refinement of the neutron diffraction pattern by the Rietveld method. [b] Calculated from the structural parameters obtained from the refinement of the X-ray and neutron diffraction patterns by the Rietveld method.

3.1.2. Magnetic Study. Numerous reports on the $Li_{1-z}Ni_{1+z}O_2$ system have already pointed out the relationship between the amount of extra nickel ions in the lithium site and the magnetic properties.[25−29] Indeed, strong antiferromagnetic interactions occur between the extra nickel ions present in the lithium site and the adjacent Ni^{2+} and Ni^{3+} ions of the slab, leading to locally ferrimagnetic clusters.[27,30] As shown by Barra et al., the size and number of clusters increase with the amount of extra nickel ions in the lithium site, so that the magnetic behavior evolves from paramagnetic order for isolated clusters to general ferrimagnetic order when all of the clusters percolate.[27,30]

The purpose of this magnetic study was not to make an overall magnetic characterization of these $LiNi_{1-y}Ti_yO_2$ phases, but only to confirm the results found for the cationic distributions by Rietveld refinement of their X-ray and neutron powder diffraction patterns, by using the sensitivity of the magnetic properties to the cluster

(21) Pouillerie, C.; Suard, E.; Delmas, C. *J. Solid State Chem.* **2001**, *158*, 187.
(22) Hagenmuller, P.; Lecerf, A.; Onillon, M. *C. R. Acad. Sci.* **1962**, *255*, 928.
(23) Maazaz, A.; Delmas, C.; Hagenmuller, P. *J. Inclusion Phenom.* **1983**, *1*, 45.
(24) Prado, G.; Suard, E.; Fournès, L.; Delmas, C. *J. Mater. Chem.* **2000**, *10*, 2553.
(25) Shirakami, T.; Takematsu, M.; Hirano, A.; Kanno, R.; Yamaura, K.; Takano, M.; Atake, T. *Mater. Sci. Eng.* **1998**, *B54*, 70.
(26) Takematsu, M.; Kawaji, H.; Atake, T.; Shirakami, T.; Hirano, A.; Kanno, R. *Electrochemistry* **2000**, *68*, 465.
(27) Barra, A. L.; Chouteau, G.; Stepanov, A.; Rougier, A.; Delmas, C. *Eur. Phys. J. B* **1999**, *7*, 551.
(28) Rougier, A.; Delmas, C.; Chouteau, G. *J. Phys. Chem. Solids* **1996**, *57*, 1101.
(29) Reimers, J. N.; Dahn, J. R.; Greedan, J. E.; Stager, C. V.; Liu, G.; Davidson, I.; von Sacken, U. *J. Solid State Chem.* **1993**, *102*, 542.
(30) Mertz, D.; Ksari, Y.; Celestini, F.; Debierre, J. M.; Stepanov, A.; Delmas, C. *Phys. Rev. B* **2000**, *61*, 1240.

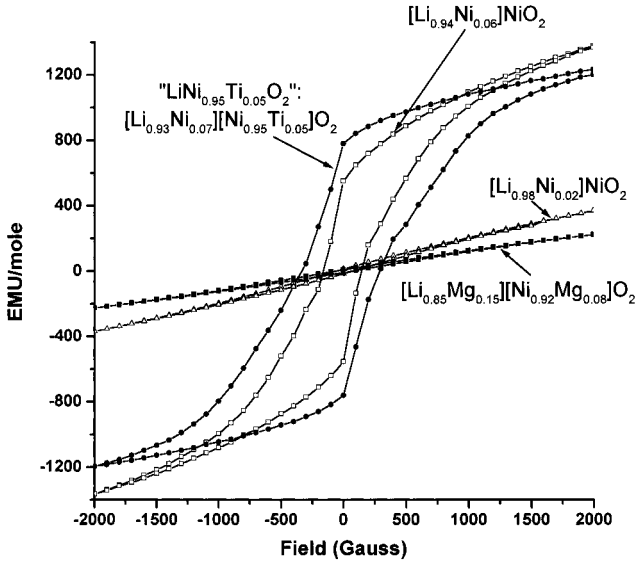

Figure 6. Comparison of the hysteresis loops recorded at 5 K for $LiNi_{0.95}Ti_{0.05}O_2$, $[Li_{0.98}Ni_{0.02}]NiO_2$, $[Li_{0.94}Ni_{0.06}]NiO_2$, and $[Li_{0.85}Mg_{0.15}][Ni_{0.92}Mg_{0.08}]O_2$.

concentration, which is directly related to the amount of paramagnetic ions in the lithium site.

Magnetization hysteresis loops were recorded at 5 K as a function of the magnetic field between −2000 and +2000 G (in steps of 100 G) to investigate the possible existence of ferromagnetic interactions in these $LiNi_{1-y}Ti_yO_2$ materials. As shown in Figure 6, a comparison of the $LiNi_{0.95}Ti_{0.05}O_2$ hysteresis loop is made with the results recorded for $[Li_{0.98}Ni_{0.02}]NiO_2$ and $[Li_{0.94}Ni_{0.06}]NiO_2$, characterized by the presence of 0.02 and 0.06 Ni^{2+} ions in the lithium site, respectively, and for $[Li_{0.85}Mg_{0.15}][Ni_{0.92}Mg_{0.08}]O_2$. It is well-known that the magnetic behavior of compounds exhibiting a significant lithium deficiency compensated by the presence of paramagnetic ions in the interslab space is quite different from that of compounds whose lithium deficiencies are not compensated in this manner.[27] Indeed, as the amount of extra paramagnetic ions in the lithium site increases, the magnetization isotherms exhibit stronger curvatures with residual magnetization at $H = 0$.[27] The residual magnetization observed at $H = 0$ for $LiTi_{0.05}Ni_{0.95}O_2$ is characteristic of ferromagnetic interactions and, therefore, confirms (as for $[Li_{0.94}Ni_{0.06}]NiO_2$) the presence of extra Ni^{2+} paramagnetic ions in the interslab space, with the Ti^{4+} ions being diamagnetic. Note that the hysteresis loops observed for $LiNi_{0.95}Ti_{0.05}O_2$ and $[Li_{0.94}Ni_{0.06}]NiO_2$ are quite similar, in good agreement with the very similar cationic distributions found by Rietveld refinement of their X-ray and neutron diffraction patterns: $[Li_{0.94}Ni^{2+}_{0.06}]_{3b}[Ni^{2+}_{0.06}Ni^{3+}_{0.94}]_{3a}$ (i.e., 0.06 ferrimagnetic clusters) and $[Li_{0.93}Ni^{2+}_{0.07}]_{3b}[Ti^{4+}_{0.05}Ni^{2+}_{0.12}Ni^{3+}_{0.83}]_{3a}$ (i.e., 0.07 ferrimagnetic clusters), respectively. Note that almost ideal paramagnetic behavior is found for $[Li_{0.98}Ni_{0.02}]NiO_2$ and $[Li_{0.85}Mg_{0.15}][Ni_{0.92}Mg_{0.08}]O_2$ because only a very small amount of Ni^{2+} ions (<2%) is present in the interslab space for the first compound and only Mg^{2+} diamagnetic ions are present in the interslab space for the second compound, to a first approximation. Such behavior would be expected for the $LiNi_{1-y}Ti_yO_2$ materials with the presence of Ti^{4+} ions in the lithium site to compensate for the lithium deficiency.

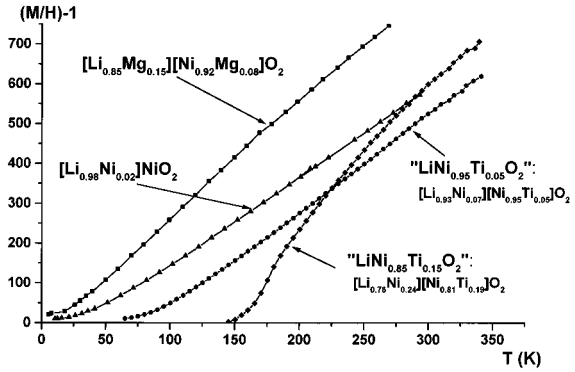

Figure 7. Variation of the reciprocal molar (M/H) ratio versus temperature for $LiNi_{0.95}Ti_{0.05}O_2$, $LiNi_{0.85}Ti_{0.15}O_2$, $[Li_{0.98}Ni_{0.02}]NiO_2$, and $[Li_{0.85}Mg_{0.15}][Ni_{0.92}Mg_{0.08}]O_2$.

Another way of describing the onset of ferromagnetic interactions is to study the magnetization as a function of temperature for these compounds at low field (here, $H = 500$ G). The variation of the reciprocal molar (M/H) ratio as a function of temperature is reported in Figure 7 for $LiNi_{0.95}Ti_{0.05}O_2$ and $LiNi_{0.85}Ti_{0.15}O_2$. The curves for $[Li_{0.98}Ni_{0.02}]NiO_2$ and $[Li_{0.85}Mg_{0.15}][Ni_{0.92}Mg_{0.08}]O_2$ are also provided for comparison. All of the curves exhibit an overall similar shape: the reciprocal molar (M/H) ratio decreases upon cooling and become equals to zero in the 0−150 K temperature range, revealing the existence of a transition temperature. The change in the curve slope in the vicinity of this temperature is weak for $LiNi_{0.95}Ti_{0.05}O_2$, indicating the appearance of short-range magnetic ordering. For $LiNi_{0.85}Ti_{0.15}O_2$, one observes a more abrupt change in the curve slope in the vicinity of the transition temperature (146 K), in agreement with a long-range ferrimagnetic behavior; for this material, the cluster concentration (23%) is larger than the critical value of 19% that leads to a cluster percolation and that was calculated using a Monte Carlo technique.[30]

This magnetic study and especially the magnetization measurements vs field at 5 K have confirmed the nature of the extra ions present in the lithium site. Indeed, these $LiNi_{1-y}Ti_yO_2$ materials are characterized by "large" residual magnetizations at $H = 0$, in good agreement with the presence of Ni^{2+} paramagnetic ions in the interslab space.

3.2. Electrochemical Study of the Li$||$$Li_xNi_{1-y}Ti_yO_2$ System (with $y = 0.05$ and 0.10). A general electrochemical study was carried out to determine the effect of titanium substitution on the electrochemical behavior of $Li_xNi_{1-y}Ti_yO_2$ ($y = 0.05$ and 0.10) as positive electrode materials for lithium batteries. In the following, the true formulas deduced for these materials from the analysis of their X-ray and neutron diffraction patterns by Rietveld refinement will be used. These formulas are $Li_{0.93}Ni_{1.02}Ti_{0.05}O_2$ and $Li_{0.86}Ni_{1.03}Ti_{0.11}O_2$ for $LiNi_{0.95}Ti_{0.05}O_2$ and $LiNi_{0.90}Ti_{0.10}O_2$, respectively.

Figures 8 and 9 show the variation of the cell voltage with the amount of lithium during the first cycles [at the *C*/20 (Figure 8) and *C*/100 (Figure 9) rates] obtained for the two titanium-substituted lithium nickelates. Note that a good reversibility of the cycling process is observed at the *C*/20 rate (Figure 8). After 14 cycles in the 3−4.6 V potential range, the reversible capacities are still equal to 144 and 111 mA h/g for $Li_{0.93}Ni_{1.02}$-

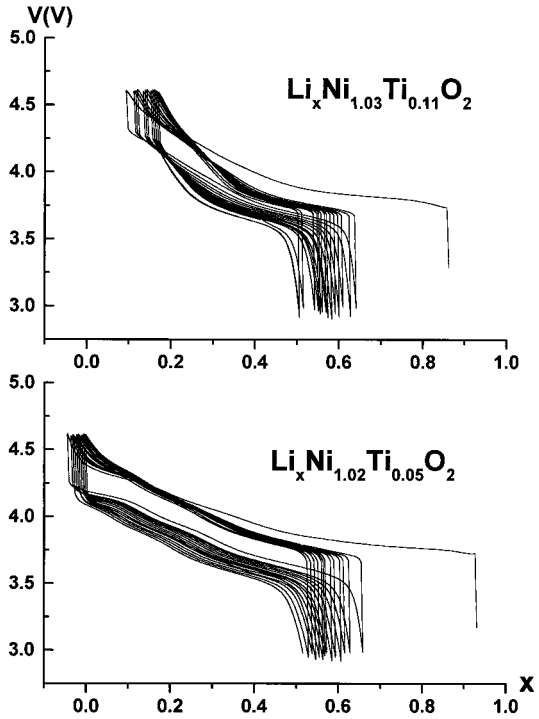

Figure 8. Variation of the cell voltage versus lithium amount at the *C*/20 rate for $Li_{0.93}Ni_{1.02}Ti_{0.05}O_2$ and $Li_{0.86}Ni_{1.03}Ti_{0.11}O_2$.

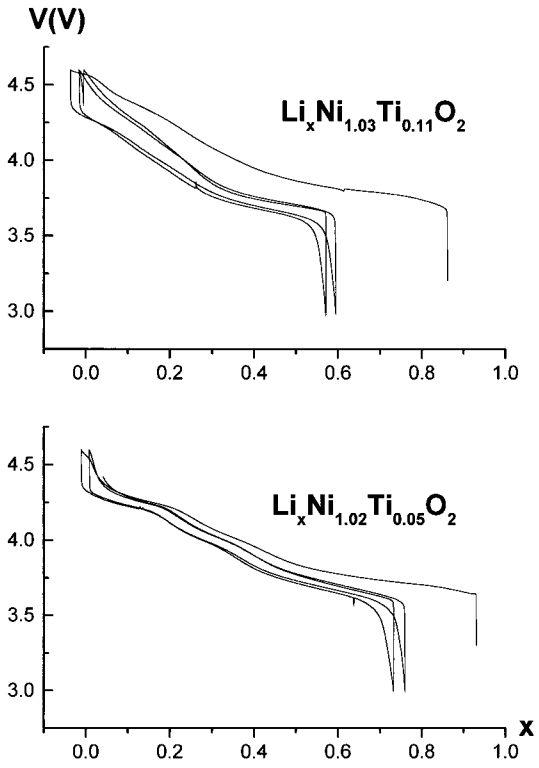

Figure 9. Variation of the cell voltage versus lithium amount at the *C*/100 rate for $Li_{0.93}Ni_{1.02}Ti_{0.05}O_2$ and $Li_{0.86}Ni_{1.03}Ti_{0.11}O_2$.

$Ti_{0.05}O_2$ and $Li_{0.86}Ni_{1.03}Ti_{0.11}O_2$, respectively. For the low cycling rate (*C*/100), all of the lithium ions can be deintercalated from the structure, which corresponds in this case to discharge capacities of ~155 and 210 mA h/g for $Li_{0.93}Ni_{1.02}Ti_{0.05}O_2$ and $Li_{0.86}Ni_{1.03}Ti_{0.11}O_2$, respectively (Figure 9). Indeed, the capacity in charge is limited by the number of lithium ions; for instance, 1.28 electrons are available for cation oxidation in $Li_{0.86}Ni_{1.03}Ti_{0.11}O_2$, whereas only 0.86 Li^+ ions can be deintercalated. The irreversible capacity observed at the end of the first cycle and the cell polarization increase with the amount of titanium in the compound, in good agreement with an increase of the amount of extra nickel ions in the interslab space. As was previously reported for the $Li_{1-z}Ni_{1+z}O_2$ system, the amount, *z*, of extra nickel ions present in the lithium site strongly affects the electrochemical properties of the materials; indeed, the irreversible oxidation of the extra nickel ions during the first charge induces a local collapse of the structure and hinders not only lithium diffusion in the interslab space but also lithium re-intercalation in the vicinity (six sites) around each nickel ion.[31] For the titanium-substituted lithium nickelates ($y \geq 0.05$), the potential−composition curves become almost monotonic, as also pointed out by the shape of the $-dx/|dV| = f(V)$ incremental capacity curves displayed in Figure 10. In comparison to the curve for $Li_{0.98}Ni_{1.02}O_2$, these curves are almost flat, thus suggesting the existence of a solid-solution domain over the entire intercalation−deintercalation composition range, which was confirmed by a detailed XRD characterization of the partially deintercalated phases obtained during the first charge.

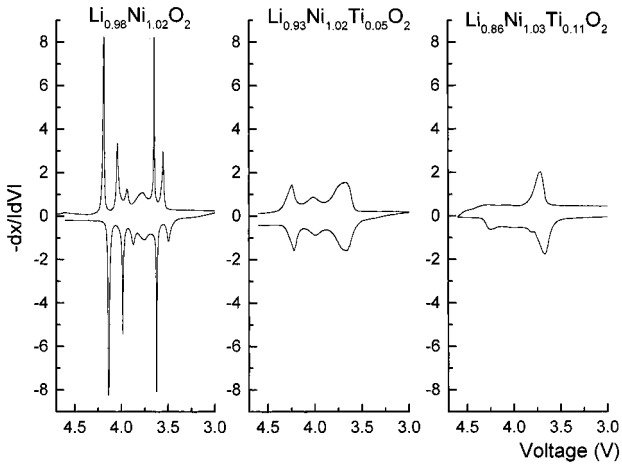

Figure 10. $-dx/|dV|$ incremental capacity curves versus voltage for $Li_{0.93}Ni_{1.02}Ti_{0.05}O_2$ and $Li_{0.86}Ni_{1.03}Ti_{0.11}O_2$, in comparison with the results obtained for $Li_{0.98}Ni_{1.02}O_2$.

Figure 11 presents as an example the XRD patterns of the $Li_xNi_{1.03}Ti_{0.11}O_2$ deintercalated phases. As was also observed for $Li_xNi_{1.02}Ti_{0.05}O_2$, only a continuous shift of the XRD lines is observed as a function of lithium composition, in agreement with the existence of a solid solution. All of these phases are isotypic with the nondeintercalated phase, i.e., characterized by an oxygen packing of the O3 type (AB CA BC) (space group $R\bar{3}m$). The cationic disordering in the slab and the presence of extra nickel ions in the interslab space, both induced by partial substitution of titanium for nickel, prevent the electronic (Ni^{3+}/Ni^{4+}) and ionic (lithium/vacancy) orderings that are at the origin of the phase transitions observed for the Li_xNiO_2 system.[32−34]

(31) Delmas, C.; Pérès, J. P.; Rougier, A.; Demourgues, A.; Weill, F.; Chadwick, A.; Broussely, M.; Perton, F.; Biensan, P.; Willmann, P. *J. Power Sources* **1997**, *68*, 120.

(32) Pérès, J. P.; Weill, F.; Delmas, C. *Solid State Ionics* **1999**, *116*, 19.

(33) Delmas, C.; Ménétrier, M.; Croguennec, L.; Levasseur, S.; Pérès, J. P.; Pouillerie, C.; Prado, G.; Fournès, L.; Weill, F. *Int. J. Inorg. Mater.* **1999**, *1*, 11.

(34) Arroyo de Dompablo, M. E.; Marianetti, C.; van der Ven, A.; Ceder, G. *Phys. Rev. B* **2001**, *63*, 144107

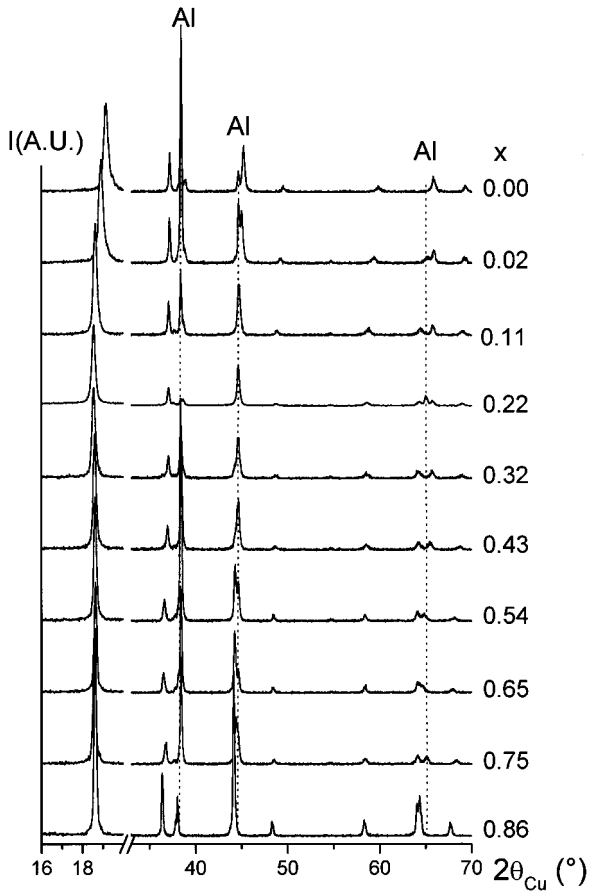

Figure 11. X-ray diffraction patterns of the $Li_xNi_{1.03}Ti_{0.11}O_2$ deintercalated phases (Al sample holder).

Figure 12 shows the variation of the hexagonal cell parameters of the deintercalated $Li_xNi_{1.02}Ti_{0.05}O_2$ and $Li_xNi_{1.03}Ti_{0.11}O_2$ phases in comparison with that for the $Li_xNi_{1.02}O_2$ system. For $x > 0.3$, the variation of the cell parameters with the amount of lithium (x) corresponds to that observed classically in layered oxides.[35,36] Indeed, a decrease of a_{hex} due to the nickel oxidation and an increase of c_{hex} due to the increase of the oxygen−oxygen electrostatic repulsions through the interslab space occur when lithium ions are removed from the structure. For the highly deintercalated phases ($x < 0.3$), a decrease of c_{hex} is observed, showing that the structure becomes covalent enough for the steric effects to prevail over the electrostatic ones.[36] In contrast to what is observed for the $Li_xNi_{1.02}O_2$ system, a continuous decrease of c_{hex} occurs at the end of the charge process for the titanium-substituted lithium nickelates, in agreement with the existence of a solid-solution reaction over the entire composition range. Note that the amplitude of this decrease is reduced when the amount of extra nickel ions increases in the interslab space because these ions play the role of pillars. At the end of the charge process, there is no formation of the O1-type structure (AB oxygen packing) as was previously observed for the $LiCoO_2$ and $LiNiO_2$ systems.[36−38] Indeed, the extra nickel ions present in the interslab space

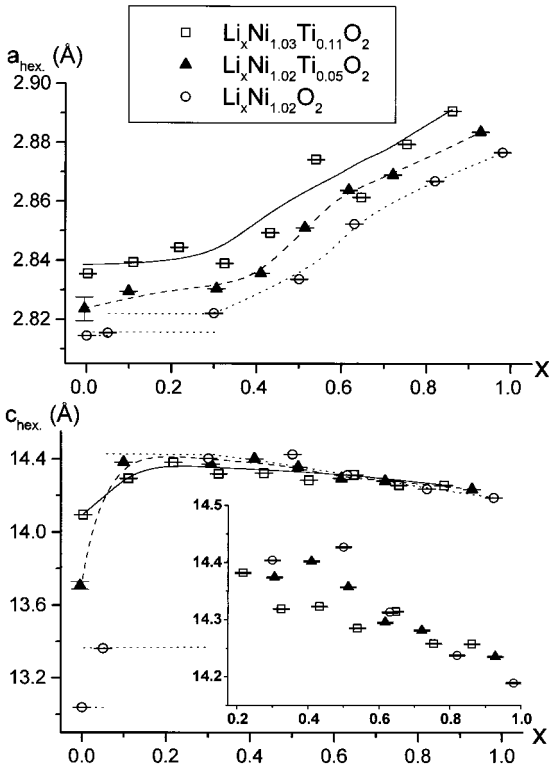

Figure 12. Variation of the hexagonal cell parameters versus lithium amount for the $Li_xNi_{1.02}Ti_{0.05}O_2$ and $Li_xNi_{1.03}Ti_{0.11}O_2$ phases, in comparison with the results observed for the $Li_xNi_{1.02}O_2$ system.

destabilize the O1-type packing in which the NiO_6 octahedra of the slab and the interslab space share faces.[36]

4. Conclusion

The characterization of the $LiNi_{1-y}Ti_yO_2$ materials by X-ray and neutron diffraction and magnetic measurements has shown that substitution of titanium for nickel in $LiNiO_2$ leads to cationic distributions such as $(Li_{1-z}Ni^{2+}_z)_{3b}(Ti^{4+}_tNi^{2+}_{t+z}Ni^{3+}_{1-z-2t})_{3a}O_2$, with the lithium deficiency being compensated by the presence of extra Ni^{2+} ions in the interslab space. As expected, there is a decrease of the reversible capacity with an increase in the amount of titanium in the lithium nickelate. Indeed, the irreversible oxidation of the extra nickel ions during the first charge induces a local collapse of the interslab space and hinders not only lithium diffusion in the interslab space but also lithium re-intercalation around each nickel ion.

A study of the thermal stability of these partially deintercalated titanium-substituted lithium nickelate compounds is now in progress, with the first results showing enhanced thermal stability in the delithiated state.

Acknowledgment. The authors thank Institut Laue-Langevin (ILL, Grenoble, France) for the neutron diffraction experiments, B. Delatouche for technical support, and CNES and Région Aquitaine for financial support.

CM011265V

(35) Pérès, J. P. Ph.D. Thesis, University of Bordeaux I, Bordeaux, France, 1996.
(36) Croguennec, L.; Pouillerie, C.; Mansour, A. N.; Delmas, C. *J. Mater. Chem.* **2001**, *11*, 131.
(37) Amatucci, G. G.; Tarascon, J. M.; Klein, L. C. *J. Electrochem. Soc.* **1996**, *143*, 1114.
(38) Arai, H.; Sakurai, Y. *Mater. Res. Soc. Symp. Proc.* **2000**, *575*, 3.